

# Origin of Open-Circuit Voltage Losses in Perovskite Solar Cells Investigated by Surface Photovoltage Measurement

Matyas Daboczi,<sup>†</sup> Iain Hamilton,<sup>†</sup> Shengda Xu,<sup>‡</sup> Joel Luke,<sup>†</sup> Saurav Limbu,<sup>†</sup> Jinho Lee,<sup>§,||</sup> Martyn A. McLachlan,<sup>‡</sup> Kwanghee Lee,<sup>||</sup> James R. Durrant,<sup>§</sup> Iain D. Baikie,<sup>⊥</sup> and Ji-Seon Kim<sup>\*,†</sup>

<sup>†</sup>Department of Physics and Centre for Plastic Electronics, <sup>‡</sup>Department of Materials and Centre for Plastic Electronics, and <sup>§</sup>Department of Chemistry and Centre for Plastic Electronics, Imperial College London, London SW7 2AZ, U.K.

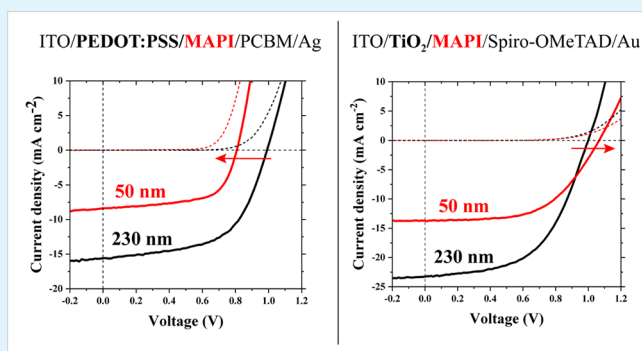
<sup>||</sup>Heeger Center for Advanced Materials and Research Institute for Solar and Sustainable Energies, Gwangju Institute of Science and Technology, Gwangju 61005, Republic of Korea

<sup>⊥</sup>KP Technology, Burn Street, Wick KW1 5EH, Caithness, U.K.

## Supporting Information

**ABSTRACT:** Increasing the open-circuit voltage ( $V_{oc}$ ) is one of the key strategies for further improvement of the efficiency of perovskite solar cells. It requires fundamental understanding of the complex optoelectronic processes related to charge carrier generation, transport, extraction, and their loss mechanisms inside a device upon illumination. Herein, we report the important origin of  $V_{oc}$  losses in methylammonium lead iodide perovskite (MAPI)-based solar cells, which results from undesirable positive charge (hole) accumulation at the interface between the perovskite photoactive layer and the poly(3,4-ethylenedioxythiophene):poly(styrenesulfonate) (PEDOT:PSS) hole-transport layer. We show strong correlation between the thickness-dependent surface photovoltage and device performance, unraveling that the interfacial charge accumulation leads to charge carrier recombination and results in a large decrease in  $V_{oc}$  for the PEDOT:PSS/MAPI inverted devices (180 mV reduction in 50 nm thick device compared to 230 nm thick one). In contrast, accumulated positive charges at the  $TiO_2$ /MAPI interface modify interfacial energy band bending, which leads to an increase in  $V_{oc}$  for the  $TiO_2$ /MAPI conventional devices (70 mV increase in 50 nm thick device compared to 230 nm thick one). Our results provide an important guideline for better control of interfaces in perovskite solar cells to improve device performance further.

**KEYWORDS:** perovskite, solar cell, open-circuit voltage, voltage loss, surface photovoltage



Exceptionally fast improvement in the power conversion efficiency (PCE) of perovskite solar cells has been achieved in the last 10 years.<sup>1–7</sup> The highest-performing perovskite devices have been reported to show PCEs above 20% with short circuit current densities ( $J_{sc}$ ) exceeding 24.5 mA cm<sup>-2</sup> and open-circuit voltages ( $V_{oc}$ ) of 1.10 V.<sup>6,7</sup> Compared to the theoretical limit of PCE, which is above 30% for an ideal semiconductor (with an optical bandgap of 1.6 eV), it is clear that the  $J_{sc}$  have almost reached their limit of 25 mA cm<sup>-2</sup>, but the  $V_{oc}$  still require further improvement<sup>8–10</sup> to meet the theoretically achievable value of 1.32 V.<sup>11,12</sup>

The conventional device structure (n–i–p-type) of perovskite solar cells often contains titanium dioxide ( $TiO_2$ ) as the electron-transport layer (ETL).<sup>13</sup> Great effort has been devoted to achieve  $V_{oc}$  higher than 1.2 V in this structure by modifying the interfacial properties between the ETL and perovskite photoactive layer. This can be achieved by changing the chemical composition of the perovskite layer<sup>14,15</sup> or changing the ETL to other oxide materials such as tin oxide for

better interfacial energy band alignment.<sup>16,17</sup> Low doping levels of the hole-transport layer (HTL) were also shown to be beneficial yielding a  $V_{oc}$  of 1.23 V.<sup>18</sup> On the other hand, in the inverted perovskite device structure (p–i–n-type), poly(3,4-ethylenedioxythiophene):poly(styrenesulfonate) (PEDOT:PSS) is commonly used as the HTL. In these devices, trap state passivation of the perovskite layer has been reported to play an important role in improving the device efficiency but without any noticeable changes in  $V_{oc}$  (1.0 V).<sup>19</sup> Instead, changing PEDOT:PSS to different types of HTLs, for example, CuSCN or polymeric HTLs have proven to improve  $V_{oc}$  up to 1.11 V.<sup>20–22</sup> Recently, with further optimization of both the low-level doped HTL and the perovskite photoactive layer to reduce nonradiative interfacial recombination, the highest  $V_{oc}$  of 1.26 V was reached.<sup>23</sup> These results highlight the important

Received: September 10, 2019

Accepted: November 18, 2019

Published: November 18, 2019

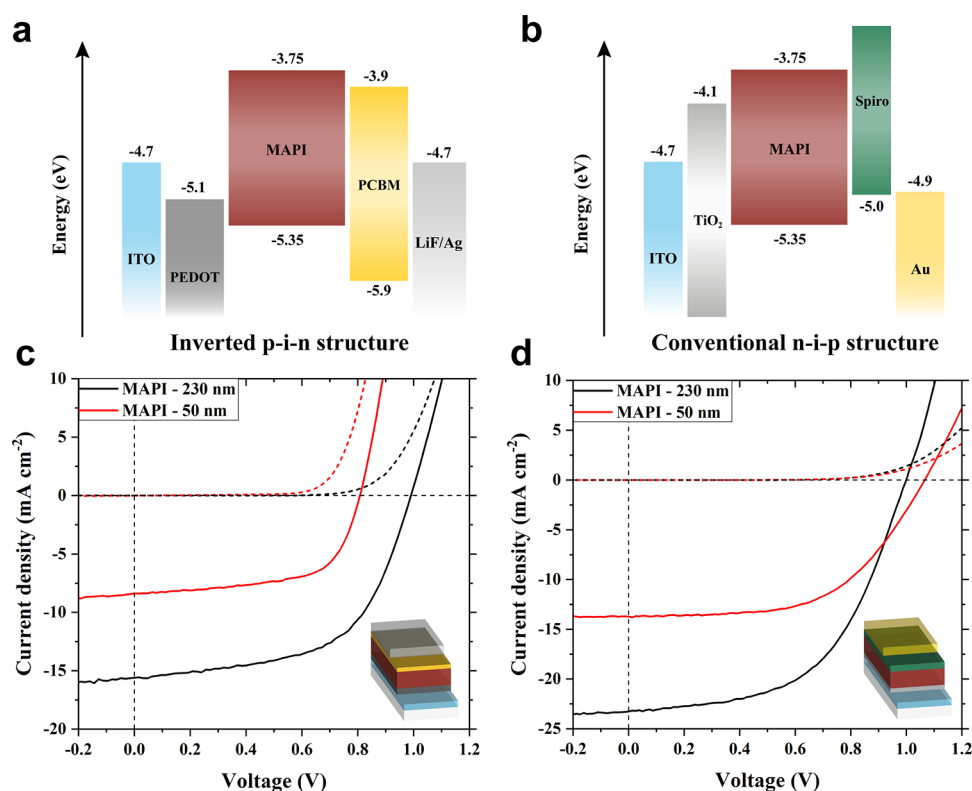


**Figure 1.** Structure and performance of perovskite devices. (a) Schematic energy band diagram of an inverted perovskite solar cell with PEDOT:PSS hole-transport layer and (b) of a conventional structure device applying TiO<sub>2</sub> electron-transport layer. (c) Reverse current–voltage scan of the inverted cell and (d) of the conventional structure device for thin (50 nm, red curve) and thick (230 nm, black curve) perovskite layers. Solid lines show scans under 1 sun equivalent illumination, while dashed lines are the corresponding dark current–voltage curves.

role of the charge-transport layers and their interfaces on the generation and loss of  $V_{oc}$  when in contact with the perovskite photoactive layer. Although many approaches have proven to be beneficial to improve  $V_{oc}$ , fundamental understanding of the physical origin of such improvements is still needed to reach device efficiency close to the radiative limit of perovskite solar cells. In this study, we aim to provide this fundamental understanding of  $V_{oc}$  by unraveling the origin of its loss in perovskite solar cells in both conventional and inverted device structures. For this, we utilize surface photovoltage measurement performed on the perovskite photoactive layer with different thicknesses deposited directly on top of TiO<sub>2</sub> and PEDOT:PSS transport layers. The measured surface photovoltage values were compared to thickness-dependent device performance to identify the origin of  $V_{oc}$  changes.

Surface photovoltage (SPV) is a contactless technique used to monitor changes in surface potential induced by generation and redistribution of photoexcited charge carriers under super-bandgap illumination.<sup>24,25</sup> The driving force for such charge redistribution is an internal electric field in the device, represented as band bending of energy levels, originating from the different Fermi levels of ETL, HTL, and perovskite layers. In a device containing sequentially deposited thin layers, the energy bands are serially connected.<sup>26</sup> Consequently, SPV, despite measuring the potential at the surface, can reveal information on the nature of bulk, surface, and interfacial properties and processes of organic and inorganic systems including charge carrier accumulation, recombination, trap states, and charge carrier decay dynamics. It has been shown for both organic<sup>27</sup> and perovskite solar cells<sup>28</sup> that the observed SPV is closely related to  $V_{oc}$ . SPV measurements

can be used to probe semiconductor stacks layer-by-layer,<sup>29</sup> which complements transient photovoltage<sup>30</sup> and open-circuit voltage decay,<sup>31</sup> techniques that are limited to complete devices.

Herein, we present thickness-dependent perovskite solar cell performance and SPV measurements for both inverted (PEDOT:PSS and [6,6]-phenyl-C<sub>61</sub>-butyric acid methyl ester (PCBM) as hole- and electron-transport layers) and conventional (TiO<sub>2</sub> and Spiro-OMeTAD as electron and hole charge-transport layers) devices. We find that reducing the thickness of the methylammonium lead iodide (MAPI) layer from 230 to 50 nm results in a significant drop in  $V_{oc}$  (−180 mV) for the inverted devices but a  $V_{oc}$  increase (+70 mV) for the conventional devices. The thickness-dependent SPV of MAPI on PEDOT:PSS and TiO<sub>2</sub> is found to be strongly correlated to such  $V_{oc}$  changes in devices. These observations are explained by positive charge accumulation at the PEDOT:PSS/MAPI and TiO<sub>2</sub>/MAPI interfaces, which leads to undesirable charge carrier recombination resulting in a significant drop of  $V_{oc}$  for thinner devices in the former case, while plausible interfacial band bending assists larger Fermi level splitting and hence improves  $V_{oc}$  in the latter case. Our results provide critical insight into the origin and loss mechanisms of  $V_{oc}$  in perovskite solar cells and can serve as an important scientific guideline for further improvement of device performance.

## RESULTS AND DISCUSSION

**Thickness-Dependent Open-Circuit Voltage.** We examined MAPI-based solar cells with two different device structures. The first contains PEDOT:PSS HTL (referred to as “inverted p–i–n structure”), while the other applies titanium

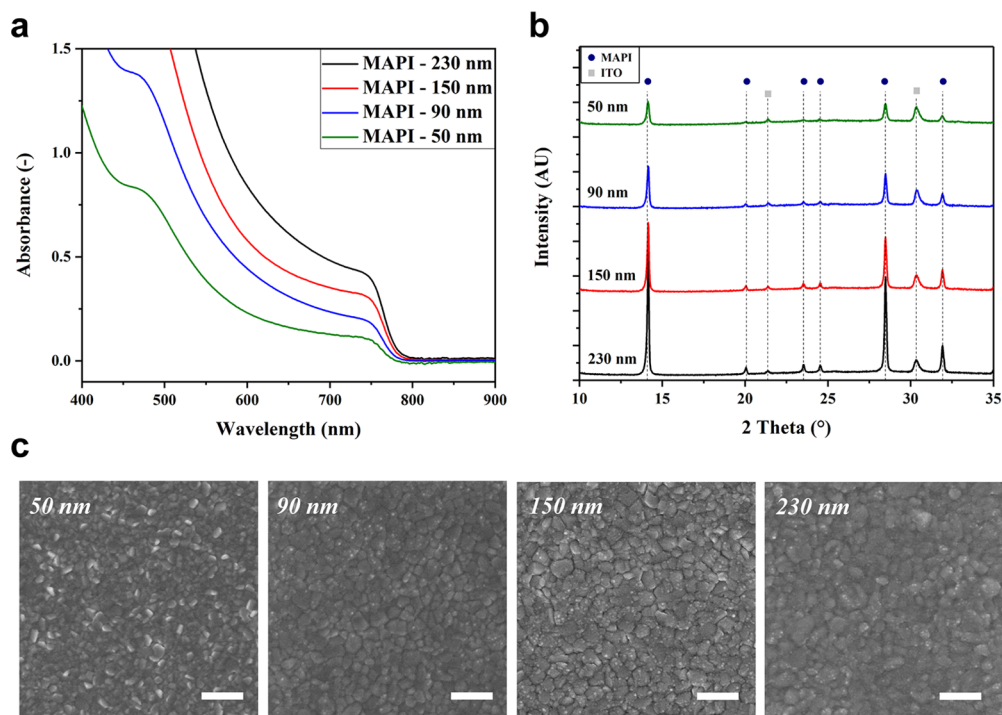


**Figure 2.** Characterization of perovskite layers with thicknesses from 230 to 50 nm. (a) UV-vis spectra, (b) X-ray diffractograms (XRD) with blue circles at MAPI peaks, and (c) scanning electron microscopy (SEM) images of MAPI layers with different thicknesses. Scale bars (SEM), 400 nm.

dioxide ( $\text{TiO}_2$ ) ETL below the photoactive perovskite layer (referred to as ‘conventional n–i–p structure’). The structure of the devices and their schematic energy band diagrams are shown in Figure 1a,b. We changed the thickness of the perovskite layer from near optimal (230 nm) to much thinner (50 nm) to investigate the effect of interfaces on the device performance. The current–voltage characteristics of the two solar cell devices (see Figure 1c,d) show that by decreasing the active layer thickness from 230 to 50 nm, the short circuit current ( $J_{sc}$ ) drops in both cases to almost half of the  $J_{sc}$  observed with the thicker MAPI layer. This is expected as the absorbance of the MAPI layer is reduced with decreasing thickness, as observed in Figure 2a. However, the devices with PEDOT:PSS HTL, regardless of MAPI layer thickness, show a  $J_{sc}$  that is over 30% lower than those that utilize a  $\text{TiO}_2$  ETL, which suggests a higher rate of charge carrier recombination in the inverted p–i–n devices.

Interestingly, the open-circuit voltage ( $V_{oc}$ ) of the inverted p–i–n structure device drops by 180 mV when decreasing the MAPI layer thickness, in contrast with the conventional n–i–p devices where  $V_{oc}$  increases by 70 mV (see Figure 1c,d). Note that there is only a small increase in fill factor in both cases ( $0.58 \pm 0.01$  to  $0.63 \pm 0.04$  and  $0.54 \pm 0.01$  to  $0.56 \pm 0.02$  for the inverted and conventional devices, respectively) indicating good surface coverage even with the thin MAPI layers. The conventional solar cells with  $\text{TiO}_2$  show significant current–voltage hysteresis, while there are only minimal differences between the forward and reverse scans of the inverted p–i–n devices applying PCBM ETL<sup>32</sup> (see Figure S1). Importantly, the thickness dependence of  $V_{oc}$  is present for reverse and forward scans for both device structures (details of photovoltaic performance and hysteresis are shown in Tables S1 and S2). The distinctly different behavior of  $V_{oc}$  as a function of MAPI layer thickness suggests different loss mechanisms of

photovoltage in the conventional and inverted device structures.

**Characterization of Perovskite Layers.** Four different thicknesses of the MAPI layer (230, 150, 90, and 50 nm) were prepared and characterized by X-ray diffraction (XRD), atomic force microscopy (AFM), and scanning electron microscopy (SEM) to rule out the potential influence of different crystallinity and morphology in the observed thickness-dependent  $V_{oc}$ . The same crystal structure for all of the thicknesses is confirmed by the X-ray diffractograms (see Figure 2b) showing for all films the same tetragonal polycrystalline MAPI diffraction peaks<sup>4,33</sup> ((001) at  $14.1^\circ$  and (220) at  $28.5^\circ$ ) without any shift in peak positions. The intensities of the MAPI diffraction peaks grow with increasing film thickness as expected, in contrast with the two decreasing indium tin oxide (ITO) substrate related peaks at  $21.4$  and  $30.3^\circ$ .<sup>34,35</sup> The AFM measurements show very similar surface roughness of the perovskite layer for all thicknesses with a calculated average root mean square roughness of  $6.1 \pm 0.5$  nm. The AFM images and corresponding line profiles are displayed in Figure S2. The SEM images of MAPI in Figure 2c show dense, pinhole-free coverage of the substrate even for the thinnest, 50 nm thick perovskite layer. SEM images for thin and thick MAPI layers on different underlayers showing very similar coverage and grain sizes can be found in Figure S3. The grain size of MAPI is in the range of 50–200 nm with smaller grains for the thinner layers (50–100 nm) and slightly larger grains (100–200 nm) for the thicker layers. The difference in grain sizes on these length scales is not expected to influence the  $V_{oc}$  of the devices as the generation and recombination of charge carriers are not significantly altered by the size and density of grains within these ranges.<sup>18</sup> We notice that the changes in grain sizes induced by different underlayers are much smaller than those induced by different thicknesses of

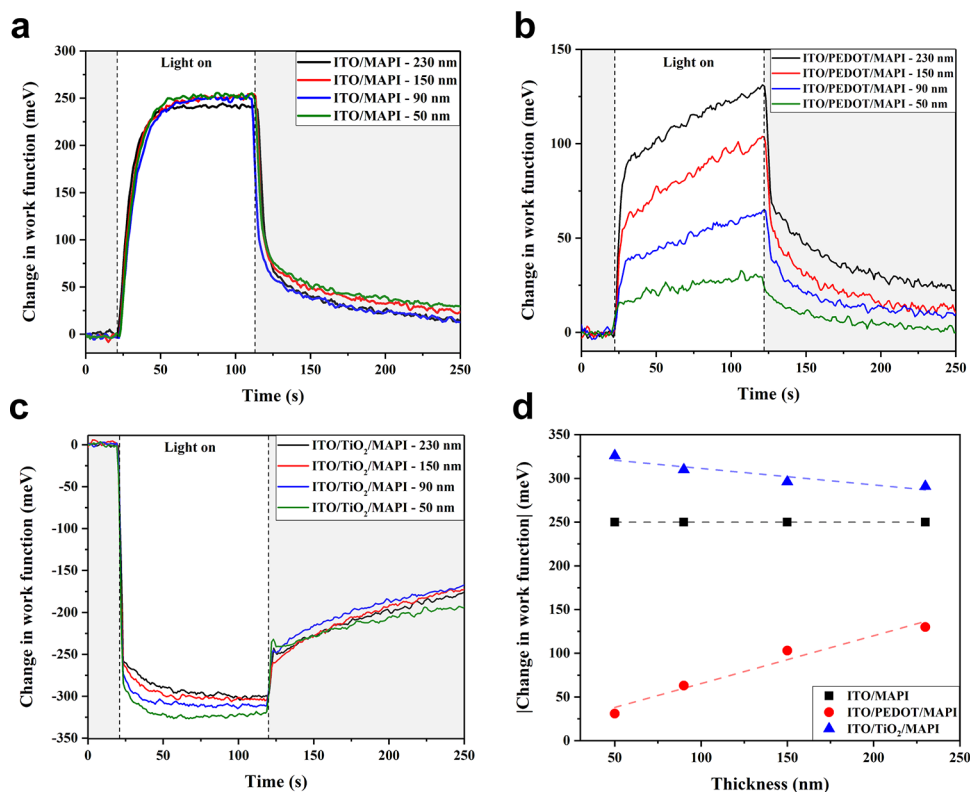


**Figure 3.** Thickness-dependent surface photovoltage measurements of MAPI. The change in work function is measured upon illumination with white light for perovskite layers with different thicknesses in the range of 230–50 nm, deposited on (a) ITO, (b) ITO/PEDOT:PSS, and (c) ITO/TiO<sub>2</sub>. Dashed vertical lines indicate when the light was turned on (first line) and off (second line). (d) The absolute value of the maximum work function changes as a function of thickness for MAPI layers deposited on ITO, PEDOT:PSS, and TiO<sub>2</sub>.

the perovskite layer, suggesting an insignificant effect of underlayer-induced grain size change on the  $V_{oc}$ .

**Energy Levels and Surface Photovoltage.** We conducted thickness-dependent energy level and surface photovoltage (SPV) measurements to understand the origin of the different behavior of  $V_{oc}$  observed in the inverted and conventional perovskite solar cells. The valence band edge of MAPI layers was measured by ambient pressure photoemission spectroscopy<sup>36</sup> at  $5.34 \pm 0.05$  eV regardless of the MAPI layer thickness or underlayers (see Figure S4). Work function values were determined in dark ( $WF_{dark}$ ) and as SPV under white light illumination ( $WF_{light}$ ). We use here the change in work function upon illumination ( $\Delta WF = WF_{light} - WF_{dark}$ ) to quantify the magnitude and sign of generated SPV.

We measured the dark work function of MAPI on both ITO and PEDOT:PSS layers at  $\sim 4.90$  eV for all thicknesses. The measured energy levels for all MAPI thicknesses are shown in Figure S5. We conclude from this result that the prepared MAPI layers are intrinsically p-type; however, the Fermi level is shifted to be shallower ( $-4.55$  eV) by the n-type TiO<sub>2</sub> as observed previously.<sup>37</sup>

The magnitude and dynamics of illumination-induced SPV for MAPI layers (from 230 to 50 nm) deposited on ITO, ITO/PEDOT:PSS, and ITO/TiO<sub>2</sub> are shown in Figure 3. Upon the formation of an interface between two materials with different Fermi energy levels (semiconductor/semiconductor or conductor/semiconductor), their Fermi energy levels will align and hence a downward band bending is expected in the lower work function semiconductor (see Figure 4a). When the semiconductor is illuminated by light with energy above the optical bandgap, photoexcited charge carriers are generated

and then redistributed in the semiconductor layer due to the band bending. This redistribution of charge carriers results in the accumulation of electrons at the surface of the top layer, reducing the band bending and leading to flat band condition at high photogenerated charge carrier density.<sup>24,29</sup> For the perovskite layers deposited on bare ITO and PEDOT:PSS, we observe a positive change in the work function, which is consistent with a downward band bending in the MAPI layer and hence an increased density of electrons at its surface under illumination.

The change in the measured work function, i.e., the magnitude of SPV, will equal the overall band bending in the sample, unless there are other processes present preventing the flat band condition to be reached under illumination (e.g., charge carrier recombination or accumulation of ions). The same magnitude (250 meV) and dynamics of SPV for all thicknesses (50–230 nm) of MAPI on ITO (see Figure 3a) imply that the band bending is the same at the ITO/MAPI interface and the width of the depletion region is shorter than 50 nm, which is expected if the ions in the perovskite layer migrate to the interface to screen the electric field.<sup>38</sup> We notice that despite the larger absorption and slightly larger grain size of the thicker (150 and 230 nm) perovskite layers (see Figure 2), the measured SPV on ITO is exactly the same as for the thinner layers, which confirms that the SPV is determined by the band bending at the ITO/MAPI interface. After the flat band condition is reached the SPV does not change any further. Even if more charge carriers are generated at higher light intensity, there is no electric field for charge redistribution therefore all generated charges recombine. This is confirmed at lower light intensities where the SPV is larger for the thick

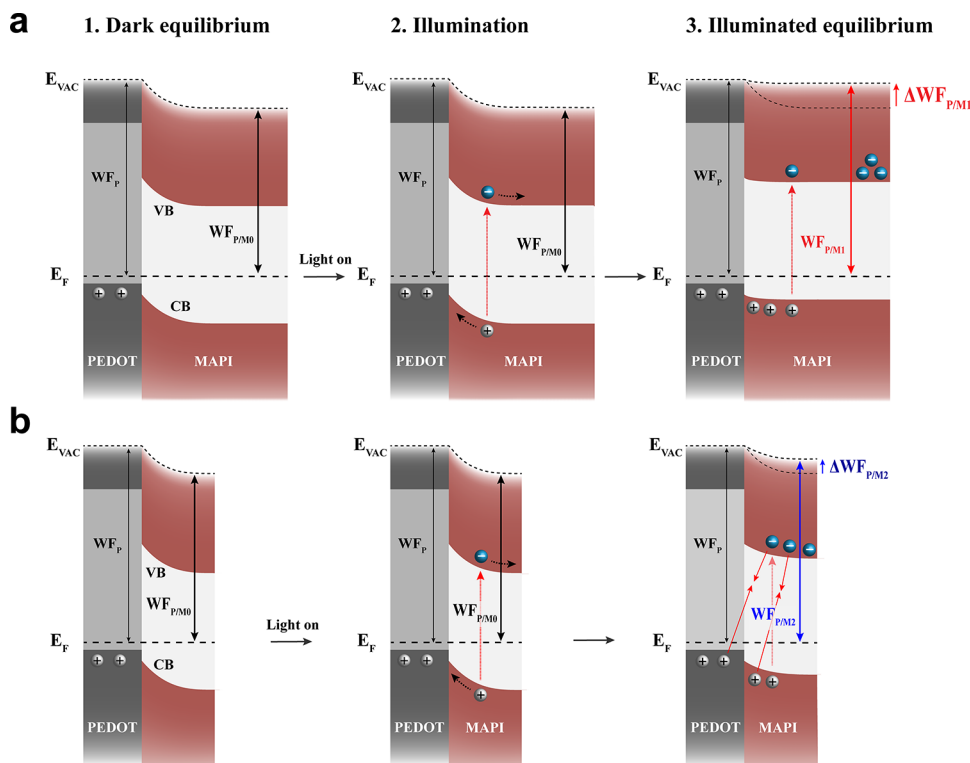


**Figure 4.** Energy band diagrams showing the generation of surface photovoltage for MAPI deposited on ITO/PEDOT:PSS. (a) Change in work function for the thick MAPI layer on PEDOT:PSS ( $\Delta WF_{P/M1}$ ) is indicated by the red arrow. (b) A smaller change in work function for a thinner MAPI layer on PEDOT:PSS ( $\Delta WF_{P/M2}$ ) is indicated by the blue arrow.  $WF_P$  denotes the work function of PEDOT:PSS,  $WF_{P/M0}$  the initial dark work function of MAPI, while  $WF_{P/M1}$  and  $WF_{P/M2}$  the work functions of MAPI under illumination for the thick and thin layers, respectively. The vacuum level, Fermi level, valence band edge, and conduction band edge are denoted by  $E_{VAC}$  (dotted line),  $E_F$  (dashed line), VB, and CB, respectively. Electrons and holes are represented by circles with negative and positive signs, respectively.

(230 nm) MAPI layer compared to the thin one (50 nm), but the difference almost disappears at higher light intensities where the SPV saturates for both thicknesses as they reach the flat band condition (see Figure S6a). It should be noted that there is a possible contribution to SPV from surface band bending<sup>39</sup> and the interfacial bending may be influenced by the presence of an interfacial dipole layer<sup>40</sup> or a selective transport layer (HTL or ETL),<sup>41,42</sup> but as the perovskite layers were prepared in an identical way and there is no difference in the measured SPV on ITO for all thicknesses, we consider these effects to be the same for all samples and, therefore, do not account for the differences observed in the thickness-dependent measurements.

The dynamics of the surface photovoltage in Figure 3 shows the presence of a slow process on the time scale of seconds when turning the light on. We attribute this to the otherwise quick processes of charge carrier transport under illumination being slowed down by the redistribution of the high density of ions in the perovskite layer,<sup>43</sup> which occurs on the seconds to hundred-seconds time scale.<sup>44</sup> We confirm this by SPV measurements at slightly increased temperatures (40 and 60 °C), where the turn-on response of the perovskite layer becomes significantly faster (the exponential lifetime ( $\tau$ ) decreases from 13 to 4 s) as the ion mobility is increased (see Figure S7). After turning the light off, the photogenerated free charge carriers can quickly recombine leading to a sharp drop in SPV ( $\tau_1 = 3-4$  s). There is an additional slower SPV decay process ( $\tau_2 = 90-120$  s), indicating potential slow recombination of trapped charge carriers<sup>45,46</sup> and redistribution of ions.<sup>47</sup>

As opposed to perovskite layers on ITO, MAPI films deposited on ITO/PEDOT:PSS show a significant reduction in the magnitude of generated SPV (see Figure 3b) with decreasing thickness of the MAPI layer. As discussed before, this variation is not due to a difference in absorption or morphology of the perovskite layer, as evidenced from the lack of thickness dependence on SPV values and dynamics measured on ITO. The slow saturation of SPV during illumination for the PEDOT:PSS/MAPI samples may be related to the relatively small magnitudes of SPV (130 meV) compared to MAPI on ITO (250 meV) and TiO<sub>2</sub> (320 meV), which means a smaller change in the electric field in MAPI and so less driving force for ion redistribution. The large density of ions in PEDOT:PSS itself might also play a role in the slow SPV saturation. The positive change in work function indicates an increased density of electrons at the surface of the perovskite layer under illumination (compared to in the dark), which results in reaching (close to) the flat band condition in the case of a thick MAPI layer, as illustrated in Figure 4a. PEDOT:PSS being a moderately selective contact for holes,<sup>41</sup> its electron blocking property is expected to be relatively weak, not being able to significantly alter the interfacial band bending and charge redistribution in the MAPI layer. In addition, due to the narrow depletion width of the MAPI as discussed above, the magnitude of band bending at the PEDOT:PSS/MAPI interface is expected to be the same for all thicknesses studied. Hence, we attribute the smaller magnitude of SPV for thinner layers of perovskite on PEDOT:PSS to recombination of photogenerated charge carriers, i.e., electrons accumulated at the surface of MAPI

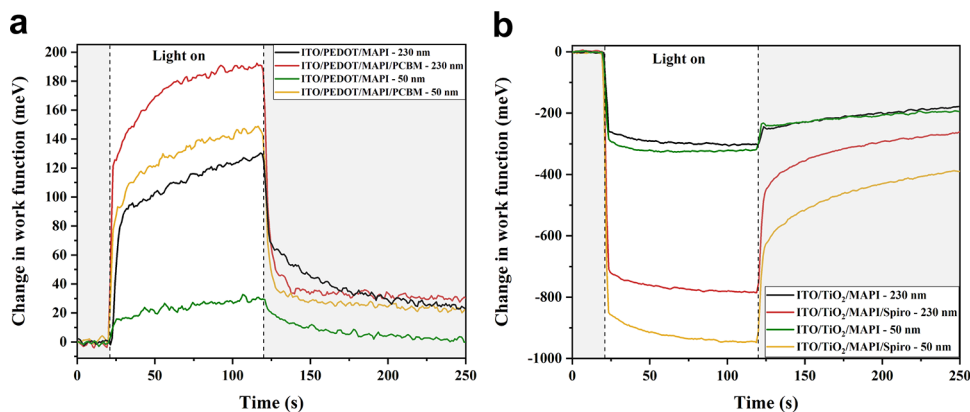


**Figure 5.** Thickness-dependent surface photovoltage measurements of MAPI with the top transport layer. Change in work function is measured upon illumination with white light for (a) ITO/PEDOT:PSS/MAPI/PCBM and (b) ITO/TiO<sub>2</sub>/MAPI/Spiro-OMeTAD with active layer thicknesses of 230 (black lines) and 50 nm (green lines). Solid/dotted lines are for samples with/without top transfer layers. Dashed vertical lines indicate when the light was turned on (first line) and off (second line).

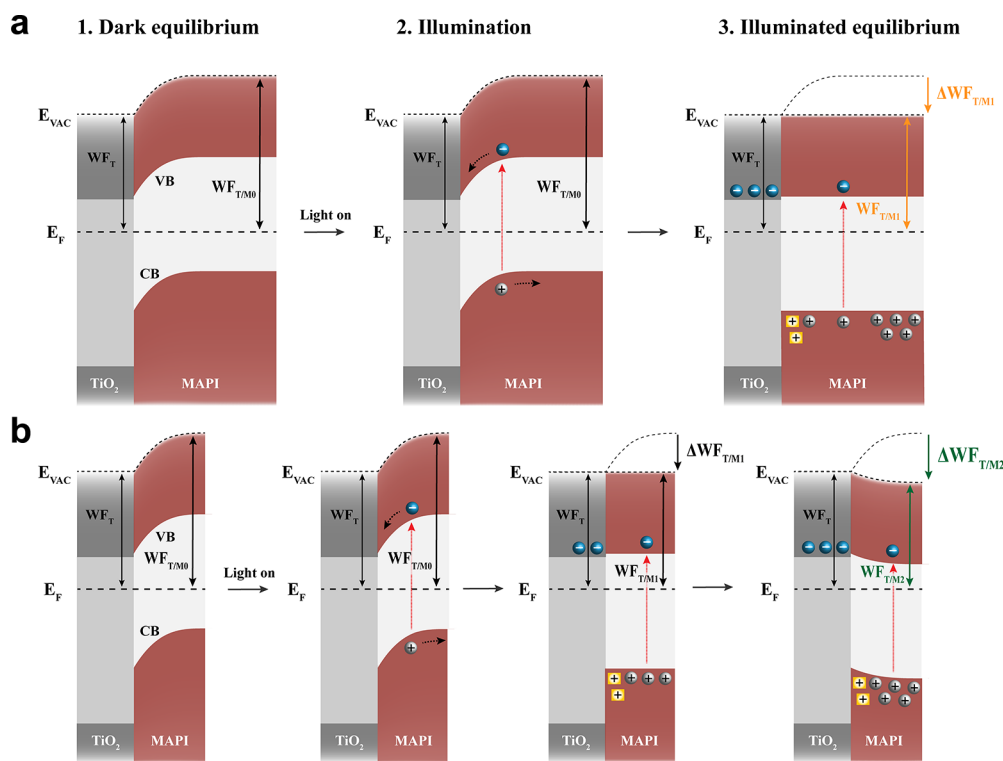


**Figure 6.** Energy band diagrams showing the generation of surface photovoltage for MAPI deposited on ITO/TiO<sub>2</sub>. (a) Change in the work function for the thick MAPI layer on TiO<sub>2</sub> ( $\Delta WF_{T/M1}$ ) is indicated by the orange arrow. (b) A larger change in the work function for a thinner MAPI layer on TiO<sub>2</sub> ( $\Delta WF_{T/M2}$ ) is indicated by the green arrow.  $WF_T$  denotes the work function of TiO<sub>2</sub>,  $WF_{T/M0}$  the initial work function of MAPI, while  $WF_{T/M1}$  and  $WF_{T/M2}$  the work functions of MAPI under illumination for the thick and thin layers, respectively. The vacuum level, Fermi level, valence band edge, and conduction band edge are denoted by  $E_{VAC}$  (dotted line),  $E_F$  (dashed line), VB, and CB, respectively. Ions are represented by squares, while photogenerated electrons and holes by circles with negative and positive signs, respectively.

recombining with holes accumulated at the PEDOT:PSS interface. Such accumulation of holes at the PEDOT:PSS/MAPI interface is possible due to significantly lower hole mobility of PEDOT:PSS<sup>48</sup> (at least two orders of magnitude smaller than that of MAPI<sup>49</sup>) and/or high density of holes in the highly doped PEDOT:PSS preventing further hole transport/extraction from the MAPI layer. This recombination of charge carriers will be more dominant with decreasing thickness of the MAPI layer due to the closer proximity of accumulated electrons and holes in thinner samples. The recombination induced SPV loss is observed in our samples; as

the thickness of the MAPI layer is reduced from 230 to 50 nm, the SPV value drops from 130 to 30 meV indicating a greater recombination rate in thinner samples (see Figure 4b).

The hole accumulation at the PEDOT:PSS/MAPI interface that leads to charge carrier recombination (proposed based on the thickness-dependent SPV measurements) can also explain the thickness-dependent  $V_{oc}$  changes observed for the inverted structure solar cells (see Figure 1a) and points to a significant loss mechanism in perovskite solar cells employing PEDOT:PSS as the HTL. To demonstrate that the proposed mechanism is also present in the full device structure in which

PEDOT:PSS and PCBM are used for the HTL and ETL, respectively, we performed SPV measurements on samples with both PEDOT:PSS and PCBM layers, as shown in Figure 5 (see repeated measurements in Figure S8). With deposition of PCBM on PEDOT:PSS/MAPI films, the magnitude of the SPV increased from 30 to 150 meV and from 130 to 190 meV for the thin (50 nm) and thick (230 nm) MAPI layers, respectively. With PCBM, the turn-on and -off response became faster without altering the sign of SPV measured (due to electrons accumulated at the top PCBM surface, see Figure 5a). These are all indications of an efficient and faster extraction of electrons through the PCBM layer. Note that the SPV value with PCBM ETL does not reach the observed  $V_{oc}$  as the silver electrode, which is expected to introduce a large band bending at the PCBM interface, is not present. Nevertheless, importantly the thickness dependence trend of SPV values still remained with PCBM, i.e., higher magnitude of SPV for the thicker film, clearly demonstrating that the recombination of photogenerated electrons with holes accumulated at the PEDOT:PSS/MAPI interface is still present.

The increase in SPV magnitude with PCBM for the thick MAPI layer is only 60 meV compared to 100 meV for the thin perovskite layer. As the thin MAPI layer has a higher recombination rate, the extraction of electrons through the PCBM layer reduces charge recombination by a greater extent than for the thick MAPI layer, leading to a larger increase in SPV. These observations corroborate the presence of charge carrier recombination due to hole accumulation at the PEDOT:PSS/MAPI interface providing a plausible explanation to the  $V_{oc}$  loss observed in thinner inverted structure MAPI devices. An accumulation of electrons at the MAPI/PCBM interface due to the low (compared to MAPI<sup>49</sup>) electron mobility of PCBM<sup>50</sup> might also play a role in the recombination as shown by varying the thickness of the PCBM layer.<sup>51</sup>

Now, we investigate the TiO<sub>2</sub>/MAPI interface. We observe a negative change in the work function under illumination for TiO<sub>2</sub>/MAPI samples, as shown in Figure 3c, opposite to the PEDOT:PSS/MAPI samples (see Figure 3d for comparison). This is expected since in the TiO<sub>2</sub>/MAPI samples, the photogenerated electrons are transported and extracted through the TiO<sub>2</sub> ETL, while the holes remain in the perovskite layer being accumulated at the surface of MAPI. TiO<sub>2</sub> has a shallower Fermi level than MAPI (see Figure S5), which leads to an upward bending in the perovskite layer at the TiO<sub>2</sub>/MAPI interface. This internal electric field under illumination drives the holes to the surface of the perovskite layer. The increasing density of holes at the surface of MAPI decreases the band bending until the flat band condition is reached (illustrated in Figure 6a), which is measured as a negative change in work function. TiO<sub>2</sub> being a strongly selective contact for electrons,<sup>42</sup> its hole blocking property is expected to be contributing to the interfacial band bending and charge redistribution of the perovskite layer. However, this phenomenon will occur at all MAPI/TiO<sub>2</sub> interfaces regardless of the MAPI layer thickness, so we do not consider it as the main factor to determine the observed thickness-dependent SPV on TiO<sub>2</sub>/MAPI samples.

When illumination is turned off, there is a small fraction (only 25%) of the fast, initial drop of SPV followed by very slow decay ( $\tau = \sim 350$  s) to reach its initial value in dark condition. This slow decay may be related to the low density of electrons being present in MAPI due to the quick and effective

electron transfer to TiO<sub>2</sub> and at the same time the excellent hole blocking property of TiO<sub>2</sub>.

Importantly, the change in work function grows (+25 meV) with decreasing thickness of MAPI on TiO<sub>2</sub> (see Figure 3c), which is opposite to the thickness-dependent SPV of MAPI on PEDOT:PSS (see comparison in Figure 3d). However, it is consistent with the increasing  $V_{oc}$  observed for conventional structure devices, as shown in Figure 1d. The difference in SPV magnitude increases even further (+150 meV), when Spiro-OMeTAD HTL is deposited on top of TiO<sub>2</sub>/MAPI samples (see Figure 5 and for repeated measurements, Figure S8) further confirming the same origin of larger SPV and  $V_{oc}$  with the thinner MAPI layer. These observations suggest that there is no significant recombination between electrons extracted to the TiO<sub>2</sub> ETL and the holes remaining in the MAPI layer. We consider that more bulk recombination in the thick layer<sup>52</sup> is not the origin of the thickness-dependent SPV of TiO<sub>2</sub>/MAPI, as that would result in lower SPV values for thicker MAPI layers on ITO as well, which we do not observe.

This interesting thickness-dependent behavior can be explained by simultaneous accumulation of both positively charged carriers (holes and ions) at the TiO<sub>2</sub>/MAPI interface, which has been suggested<sup>31</sup> based on device simulations and analysis of open-circuit voltage decays (similar to the SPV decays here) and has also been confirmed by cross-sectional Kelvin probe force microscopy measurements.<sup>46</sup> The increased density of positively charged carriers at the surface of the MAPI layer can lead to the flat band condition (see Figure 6a). The magnitude of interfacial band bending is the same for all thicknesses as discussed above, indicating that the same density of accumulated charge carriers is present at the MAPI surface when flat band condition is reached. However, these positive charge carriers would be more confined to the TiO<sub>2</sub>/MAPI interface in the thinner MAPI layer, now being able to lead to a downward (beyond flat band) bending and so a larger change in the measured work function (see Figure 6b).

The larger SPV present for the thin (50 nm) MAPI layer on TiO<sub>2</sub> compared to the thick one (230 nm, see Figure 3) and the fact that the difference in SPV magnitude increases even further when Spiro-OMeTAD HTL is deposited on top of TiO<sub>2</sub>/MAPI layers (see Figure 5) imply that accumulation of positively charged species (holes and ions) at the TiO<sub>2</sub>/MAPI interface is also present in full solar cells, and we relate it to the observed increase of  $V_{oc}$  in the conventional structure device.

Based on these findings, one can design perovskite solar cells to prevent the  $V_{oc}$  losses described above and hence to improve device performance further. For example, for the inverted structure devices, such  $V_{oc}$  losses could be avoided by reducing the doping level of the HTL, so preventing interfacial hole accumulation and charge carrier recombination.<sup>53</sup> On the other hand, for TiO<sub>2</sub>-based devices, the high density of ions (cations) could potentially be used to increase the positive charge accumulation at the TiO<sub>2</sub>/MAPI interface to improve  $V_{oc}$ .

## CONCLUSIONS

In summary, we prepared inverted (PEDOT:PSS-based) and conventional structure (TiO<sub>2</sub>-based) MAPI solar cells with different active layer thicknesses (230–50 nm) to investigate the origin of  $V_{oc}$  loss. We find that when decreasing the thickness of the perovskite layer, the  $V_{oc}$  decreases significantly (–180 mV) for the inverted devices but increases (+70 mV) for the conventional devices.

Different thicknesses of the MAPI layer on ITO show the same magnitude and dynamics of SPV, indicating that bulk MAPI defects are not the cause of the observed  $V_{oc}$  changes. However, on PEDOT:PSS HTL, the magnitude of SPV drops with decreasing the MAPI layer thickness, due to an increased accumulation of holes at the PEDOT:PSS/MAPI interface, leading to a higher rate of recombination in thin layers. Such a hole-accumulation-induced recombination is also present in the PEDOT:PSS/MAPI/PCBM structure, suggesting that it is an important origin of  $V_{oc}$  loss in the inverted device structure. In contrast, thinner MAPI layers on  $TiO_2$  ETL compared to thicker ones show a higher magnitude of SPV, which is explained by accumulation of positive charge carriers (both holes and cations) at the  $TiO_2$ /MAPI interface leading to a band banding beyond flat band under illumination.<sup>31,46</sup> Such an accumulation is also observed in the  $TiO_2$ /MAPI/Spiro-OMeTAD structure, confirming that the interfacial accumulation of positive charge carriers is responsible for the observed increase in  $V_{oc}$  for the conventional structure solar cell. These results provide new insight into the origin of open-circuit voltage in inverted and conventional structure perovskite solar cells, which will be critical when aiming to further increase device performance.

## METHODS

**Sample Preparation.** Indium tin oxide (ITO)-coated glass substrates were cleaned in ultrasonic bath sequentially in aqueous detergent solution (2% (v/v) of Hellmanex III), acetone, and 2-propanol and dried with nitrogen. Before deposition of further layers, the substrates were treated for 5 min in oxygen plasma at 80 W.

The structure was ITO/ $TiO_2$ /MAPI/Spiro-OMeTAD/Au for the conventional solar cells and ITO/PEDOT:PSS/MAPI/PCBM/LiF/Ag for the inverted devices, where MAPI is methylammonium lead iodide, Spiro-OMeTAD is 2,2',7,7'-tetrakis(*N,N*-di-*p*-methoxyphenylamine)-9,9'-spirobifluorene, and Au is gold. PEDOT:PSS stands for poly(3,4-ethylenedioxythiophene) polystyrene sulfonate, PCBM for [6,6]-phenyl- $C_{61}$ -butyric acid methyl ester, and Ag for silver.

The  $TiO_2$  layers were spin-coated on cleaned ITO at 2000 rpm from acetic (0.013 M HCl) solution of titanium isopropoxide (0.23 M, 97%, Sigma-Aldrich) in ethanol. The layers were annealed at 150 °C for 10 min and at 450 °C for 30 min. PEDOT:PSS was spun from its aqueous solution (Clevios P VP AI 4083, Heraeus) on the cleaned ITO substrate at 2500 rpm and annealed at 135 °C for 10 min. The MAPI layers with different thicknesses were prepared from 0.5, 0.75, 1.0, and 1.25 M  $\gamma$ -butyrolactone/dimethyl sulfoxide (ratio of 7:3) solution of stoichiometric ratio lead iodide (Sigma-Aldrich, 99%) and methylammonium iodide (Sigma-Aldrich, 98%), using the same spinning speed (4000 rpm) and with dripping of 500  $\mu$ L of toluene after 8 s spinning time. This resulted in around 50, 90, 150, and 230 nm thick perovskite layers after annealing them at 100 °C for 10 min. For the conventional structure devices, Spiro-OMeTAD (99.8%, Borun Technology) top transport layer was deposited from 82 mg  $mL^{-1}$  chlorobenzene solution at 3000 rpm. For doping Spiro-OMeTAD, 64 mg of bis(trifluoromethane)sulfonamide lithium salt (99.95%, Sigma-Aldrich) and 20  $\mu$ L of 4-tert-butylpyridine (96%, Sigma-Aldrich) were added to 1 mL of the solution. These devices were finished by evaporation of 80 nm gold electrode. The top transport layer for the inverted structure devices was prepared by spin-coating PCBM (Ossila) from 20 mg  $mL^{-1}$  chlorobenzene solution at 2000 rpm. The devices were finished by evaporating 1 nm LiF and 100 nm silver astop electrodes.

**Solar Cell Characterization.** The current–voltage characteristic of the perovskite devices was obtained by a Keithley 236 Source Measure Unit and a solar simulator with AM1.5G filters (Oriental Instruments). A calibrated Si photodiode (Osram BPW21) was used to adjust the light intensity on the sample to be 100  $mW\ cm^{-2}$ . First forward scan from  $-0.4$  to 1.5 V and then reverse scan was taken at

0.1  $V\ s^{-1}$  rate. The samples were not biased or illuminated before the measurements.

**Characterization of Perovskite Layers.** Absorbance of MAPI layers was calculated from transmittance and reflectance measured by a Shimadzu UV-2600 UV–vis spectrophotometer.

The crystal structure of MAPI layers was investigated by X-ray diffraction (XRD) using a PANalytical X'Pert diffractometer (Cu  $K\alpha$ ,  $l = 1.54\ \text{\AA}$ ) at 40 kV and 40 mA. The diffraction patterns were obtained over the  $2\theta$  range of 6–40° in steps of 0.034° and subsequently analyzed using the HighScore software.

Gemini LEO 1525 scanning electron microscopy was used to obtain the SEM images. Accelerating voltage was 4–5 kV, and the working distance was kept as low as possible (<5 mm). Prior to imaging, all samples were coated with 10 nm chromium.

Atomic force microscopy (AFM) topography images of the perovskite layers were obtained by a Park NX10 AFM in the noncontact mode.

**Ambient Pressure Photoemission Spectroscopy (APS) and Surface Photovoltage (SPV).** The APS and SPV measurements were performed by an APS04 system (KP Technology) on samples prepared on cleaned ITO substrates the same way as described above. During the measurements, the ITO substrate was connected to the ground.

The valence band edge of the semiconductor layers was determined by scanning the UV light excitation in the range of 4.8–6.2 eV and extrapolating the cube root photoemission to zero. Fermi level of the samples was calculated from the contact potential difference measured by the vibrating top Kelvin probe (2 mm, gold tip) and from the work function of the tip (around 4.5–4.6 eV), which was determined every day using a silver reference.

The samples were kept and prepared in the dark (or minimal light condition) for SPV measurements. Before the measurement was taken, the dark work function was monitored until a stable signal was reached. Then, the sample was illuminated with white light (20  $mW\ cm^{-2}$ ) for 100 s and the SPV decay was recorded for further 150 s.

## ASSOCIATED CONTENT

### Supporting Information

The Supporting Information is available free of charge at <https://pubs.acs.org/doi/10.1021/acsami.9b16394>.

Photovoltaic performance parameters of inverted and conventional structure devices; current–voltage hysteresis curves; AFM, SEM, and APS measurements for different MAPI layer thicknesses; energy levels measured under dark and light conditions on different underlayers; light intensity, temperature-dependent and repeated SPV measurements of MAPI perovskite layers (PDF)

## AUTHOR INFORMATION

### Corresponding Author

\*E-mail: [ji-seon.kim@imperial.ac.uk](mailto:ji-seon.kim@imperial.ac.uk).

### ORCID

Matyas Daboczi: 0000-0001-9920-3657

Iain Hamilton: 0000-0002-0685-1696

Joel Luke: 0000-0003-3208-8572

Martyn A. McLachlan: 0000-0003-3136-1661

Kwanghee Lee: 0000-0002-5907-8625

James R. Durrant: 0000-0001-8353-7345

Ji-Seon Kim: 0000-0003-4715-3656

### Notes

The authors declare no competing financial interest.

## ACKNOWLEDGMENTS

The authors would like to thank Piers R. F. Barnes and Philip Calado for all of the helpful discussions. The authors

acknowledge the funding of UK Engineering and Physical Sciences Research Council (EPSRC) Plastic Electronics Centre for Doctoral Training (EP/L016702/1) and KP Technology Ltd for a CASE studentship support. Support from the Global Research Laboratory Program of the National Research Foundation (NRF) funded by the Ministry of Science, ICT & Future Planning (NRF-2017K1A1A2013153) is greatly acknowledged.

## REFERENCES

- (1) Kojima, A.; Teshima, K.; Shirai, Y.; Miyasaka, T. Organometal Halide Perovskites as Visible-Light Sensitizers for Photovoltaic Cells. *J. Am. Chem. Soc.* **2009**, *131*, 6050–6051.
- (2) Kim, H. S.; Lee, C. R.; Im, J. H.; Lee, K. B.; Moehl, T.; Marchioro, A.; Moon, S. J.; Humphry-Baker, R.; Yum, J. H.; Moser, J. E.; et al. Lead Iodide Perovskite Sensitized All-Solid-State Submicron Thin Film Mesoscopic Solar Cell with Efficiency Exceeding 9%. *Sci. Rep.* **2012**, *2*, No. 591.
- (3) Docampo, P.; Ball, J. M.; Darwich, M.; Eperon, G. E.; Snaith, H. J. Efficient Organometal Trihalide Perovskite Planar-Heterojunction Solar Cells on Flexible Polymer Substrates. *Nat. Commun.* **2013**, *4*, No. 2761.
- (4) Liu, M.; Johnston, M. B.; Snaith, H. J. Efficient Planar Heterojunction Perovskite Solar Cells by Vapour Deposition. *Nature* **2013**, *501*, 395–398.
- (5) Saliba, M.; Matsui, T.; Seo, J. Y.; Domanski, K.; Correa-Baena, J. P.; Nazeeruddin, M. K.; Zakeeruddin, S. M.; Tress, W.; Abate, A.; Hagfeldt, A.; et al. Cesium-Containing Triple Cation Perovskite Solar Cells: Improved Stability, Reproducibility and High Efficiency. *Energy Environ. Sci.* **2016**, *9*, 1989–1997.
- (6) Shin, S. S.; Yeom, E. J.; Yang, W. S.; Hur, S.; Kim, M. G.; Im, J.; Seo, J.; Noh, J. H.; Seok, S. I. Colloidally Prepared La-Doped BaSnO<sub>3</sub> Electrodes for Efficient, Photostable Perovskite Solar Cells. *Science* **2017**, *356*, 167–171.
- (7) Yang, W. S.; Park, B. W.; Jung, E. H.; Jeon, N. J.; Kim, Y. C.; Lee, D. U.; Shin, S. S.; Seo, J.; Kim, E. K.; Noh, J. H.; et al. Iodide Management in Formamidinium-Lead-Halide-Based Perovskite Layers for Efficient Solar Cells. *Science* **2017**, *356*, 1376–1379.
- (8) Marinova, N.; Valero, S.; Delgado, J. L. Organic and Perovskite Solar Cells: Working Principles, Materials and Interfaces. *J. Colloid Interface Sci.* **2017**, *488*, 373–389.
- (9) Correa-Baena, J. P.; Abate, A.; Saliba, M.; Tress, W.; Jesper Jacobsson, T.; Grätzel, M.; Hagfeldt, A. The Rapid Evolution of Highly Efficient Perovskite Solar Cells. *Energy Environ. Sci.* **2017**, *10*, 710–727.
- (10) Tress, W. Perovskite Solar Cells on the Way to Their Radiative Efficiency Limit – Insights Into a Success Story of High Open-Circuit Voltage and Low Recombination. *Adv. Energy Mater.* **2017**, *7*, No. 1602358.
- (11) Sha, W. E. I.; Ren, X.; Chen, L.; Choy, W. C. H. The Efficiency Limit of CH<sub>3</sub>NH<sub>3</sub>PbI<sub>3</sub> Perovskite Solar Cells. *Appl. Phys. Lett.* **2015**, *106*, No. 221104.
- (12) Tress, W. Maximum Efficiency and Open-Circuit Voltage of Perovskite Solar Cells. In *Organic-Inorganic Halide Perovskite Photo-voltaics: From Fundamentals to Device Architectures*; Park, N.-G., Grätzel, M., Miyasaka, T., Eds.; Springer International Publishing: Cham, 2016; pp 53–77.
- (13) Snaith, H. J. Perovskites: The Emergence of a New Era for Low-Cost, High-Efficiency Solar Cells. *J. Phys. Chem. Lett.* **2013**, *4*, 3623–3630.
- (14) Bi, D.; Tress, W.; Dar, M. I.; Gao, P.; Luo, J.; Renevier, C.; Schenk, K.; Abate, A.; Giordano, F.; Correa Baena, J. P.; et al. Efficient Luminescent Solar Cells Based on Tailored Mixed-Cation Perovskites. *Sci. Adv.* **2016**, *2*, No. e1501170.
- (15) Jodlowski, A. D.; Roldán-Carmona, C.; Grancini, G.; Salado, M.; Ralaiarisoa, M.; Ahmad, S.; Koch, N.; Camacho, L.; De Miguel, G.; Nazeeruddin, M. K. Large Guanidinium Cation Mixed with Methylammonium in Lead Iodide Perovskites for 19% Efficient Solar Cells. *Nat. Energy* **2017**, *2*, 972–979.
- (16) Correa Baena, J. P.; Steier, L.; Tress, W.; Saliba, M.; Neutzner, S.; Matsui, T.; Giordano, F.; Jacobsson, T. J.; Srimath Kandada, A. R.; Zakeeruddin, S. M.; et al. Highly Efficient Planar Perovskite Solar Cells through Band Alignment Engineering. *Energy Environ. Sci.* **2015**, *8*, 2928–2934.
- (17) Anaraki, E. H.; Kermanpur, A.; Steier, L.; Domanski, K.; Matsui, T.; Tress, W.; Saliba, M.; Abate, A.; Grätzel, M.; Hagfeldt, A.; et al. Highly Efficient and Stable Planar Perovskite Solar Cells by Solution-Processed Tin Oxide. *Energy Environ. Sci.* **2016**, *9*, 3128–3134.
- (18) Correa-Baena, J. P.; Tress, W.; Domanski, K.; Anaraki, E. H.; Turren-Cruz, S. H.; Roose, B.; Boix, P. P.; Grätzel, M.; Saliba, M.; Abate, A.; et al. Identifying and Suppressing Interfacial Recombination to Achieve High Open-Circuit Voltage in Perovskite Solar Cells. *Energy Environ. Sci.* **2017**, *10*, 1207–1212.
- (19) Shao, Y.; Xiao, Z.; Bi, C.; Yuan, Y.; Huang, J. Origin and Elimination of Photocurrent Hysteresis by Fullerene Passivation in CH<sub>3</sub>NH<sub>3</sub>PbI<sub>3</sub>planar Heterojunction Solar Cells. *Nat. Commun.* **2014**, *5*, No. 6784.
- (20) Malinkiewicz, O.; Yella, A.; Lee, Y. H.; Espallargas, G. M.; Graetzel, M.; Nazeeruddin, M. K.; Bolink, H. J. Perovskite Solar Cells Employing Organic Charge-Transport Layers. *Nat. Photonics* **2014**, *8*, 128–132.
- (21) Lee, J.; Kang, H.; Kim, G.; Back, H.; Kim, J.; Hong, S.; Park, B.; Lee, E.; Lee, K. Achieving Large-Area Planar Perovskite Solar Cells by Introducing an Interfacial Compatibilizer. *Adv. Mater.* **2017**, *29*, 1–8.
- (22) Wijeyasinghe, N.; Regoutz, A.; Eisner, F.; Du, T.; Tsetseris, L.; Lin, Y. H.; Faber, H.; Pattanasattayavong, P.; Li, J.; Yan, F.; et al. Copper(I) Thiocyanate (CuSCN) Hole-Transport Layers Processed from Aqueous Precursor Solutions and Their Application in Thin-Film Transistors and Highly Efficient Organic and Organometal Halide Perovskite Solar Cells. *Adv. Funct. Mater.* **2017**, *27*, 1–13.
- (23) Liu, Z.; Krückemeier, L.; Krogmeier, B.; Klingebiel, B.; Márquez, J. A.; Levchenko, S.; Öz, S.; Mathur, S.; Rau, U.; Unold, T.; et al. Open-Circuit Voltages Exceeding 1.26 v in Planar Methylammonium Lead Iodide Perovskite Solar Cells. *ACS Energy Lett.* **2019**, *4*, 110–117.
- (24) Kronik, L.; Shapira, Y. Surface Photovoltage Phenomena: Theory, Experiment, and Applications. *Surf. Sci. Rep.* **1999**, *37*, 1–206.
- (25) Cavalcoli, D.; Cavallini, A. Surface Photovoltage Spectroscopy -Method and Applications. *Phys. Status Solidi C* **2010**, *7*, 1293–1300.
- (26) Kronik, L.; Shapira, Y. Surface Photovoltage Spectroscopy of Semiconductor Structures: At the Crossroads of Physics, Chemistry and Electrical Engineering. *Surf. Interface Anal.* **2001**, *31*, 954–965.
- (27) Lee, Y. J.; Wang, J.; Hsu, J. W. P. Surface Photovoltage Characterization of Organic Photovoltaic Devices. *Appl. Phys. Lett.* **2013**, *103*, No. 173302.
- (28) Harwell, J. R.; Baikie, T. K.; Baikie, I. D.; Payne, J. L.; Ni, C.; Irvine, J. T. S.; Turnbull, G. A.; Samuel, I. D. W. Probing the Energy Levels of Perovskite Solar Cells: Via Kelvin Probe and UV Ambient Pressure Photoemission Spectroscopy. *Phys. Chem. Chem. Phys.* **2016**, *18*, 19738–19745.
- (29) Lee, B. N.; Kirmayer, S.; Edri, E.; Hodes, G.; Cahen, D. Surface Photovoltage Spectroscopy Study of Organo-Lead Perovskite Solar Cells. *J. Phys. Chem. Lett.* **2014**, *5*, 2408–2413.
- (30) Wheeler, S.; Bryant, D.; Troughton, J.; Kirchartz, T.; Watson, T.; Nelson, J.; Durrant, J. R. Transient Optoelectronic Analysis of the Impact of Material Energetics and Recombination Kinetics on the Open-Circuit Voltage of Hybrid Perovskite Solar Cells. *J. Phys. Chem. C* **2017**, *121*, 13496–13506.
- (31) Gottesman, R.; Lopez-Varo, P.; Gouda, L.; Jimenez-Tejada, J. A.; Hu, J.; Tirosh, S.; Zaban, A.; Bisquert, J. Dynamic Phenomena at Perovskite/Electron-Selective Contact Interface as Interpreted from Photovoltage Decays. *Chem* **2016**, *1*, 776–789.
- (32) Xu, J.; Buin, A.; Ip, A. H.; Li, W.; Voznyy, O.; Comin, R.; Yuan, M.; Jeon, S.; Ning, Z.; McDowell, J. J.; et al. Perovskite-Fullerene

Hybrid Materials Suppress Hysteresis in Planar Diodes. *Nat. Commun.* **2015**, *6*, No. 7081.

(33) Du, T.; Burgess, C. H.; Kim, J.; Zhang, J.; Durrant, J. R.; McLachlan, M. A. Formation, Location and Beneficial Role of PbI<sub>2</sub> in Lead Halide Perovskite Solar Cells. *Sustainable Energy Fuels* **2017**, *1*, 119–126.

(34) Maruyama, T.; Fukui, K. Indium-Tin Oxide Thin Films Prepared by Chemical Vapor Deposition. *J. Appl. Phys.* **1991**, *70*, 3848–3851.

(35) Kim, H.; Gilmore, C. M.; Piqué, A.; Horwitz, J. S.; Mattoussi, H.; Murata, H.; Kafafi, Z. H.; Chrisey, D. B. Electrical, Optical, and Structural Properties of Indium-Tin-Oxide Thin Films for Organic Light-Emitting Devices. *J. Appl. Phys.* **1999**, *86*, 6451–6461.

(36) Baikie, I. D.; Grain, A. C.; Sutherland, J.; Law, J. Dual Mode Kelvin Probe: Featuring Ambient Pressure Photoemission Spectroscopy and Contact Potential Difference. *Energy Procedia* **2014**, *60*, 48–56.

(37) Miller, E. M.; Zhao, Y.; Mercado, C. C.; Saha, S. K.; Luther, J. M.; Zhu, K.; Stevanović, V.; Perkins, C. L.; Van De Lagemaat, J. Substrate-Controlled Band Positions in CH<sub>3</sub>NH<sub>3</sub>PbI<sub>3</sub>perovskite Films. *Phys. Chem. Chem. Phys.* **2014**, *16*, 22122–22130.

(38) Tress, W.; Marinova, N.; Moehl, T.; Zakeeruddin, S. M.; Nazeeruddin, M. K.; Grätzel, M. Understanding the Rate-Dependent J-V Hysteresis, Slow Time Component, and Aging in CH<sub>3</sub>NH<sub>3</sub>PbI<sub>3</sub> Perovskite Solar Cells: The Role of a Compensated Electric Field. *Energy Environ. Sci.* **2015**, *8*, 995–1004.

(39) Zhang, W.; Pathak, S.; Sakai, N.; Stergiopoulos, T.; Nayak, P. K.; Noel, N. K.; Haghighirad, A. A.; Burlakov, V. M.; Dequillettes, D. W.; Sadhanala, A.; et al. Enhanced Optoelectronic Quality of Perovskite Thin Films with Hypophosphorous Acid for Planar Heterojunction Solar Cells. *Nat. Commun.* **2015**, *6*, No. 10030.

(40) Olthof, S.; Meerholz, K. Substrate-Dependent Electronic Structure and Film Formation of MAPbI<sub>3</sub> Perovskites. *Sci. Rep.* **2017**, *7*, No. 40267.

(41) Luo, H.; Lin, X.; Hou, X.; Pan, L.; Huang, S.; Chen, X. Efficient and Air-Stable Planar Perovskite Solar Cells Formed on Graphene-Oxide-Modified PEDOT:PSS Hole Transport Layer. *Nano-Micro Lett.* **2017**, *9*, 1–11.

(42) Zhang, Y.; Liu, M.; Eperon, G. E.; Leijtens, T. C.; McMeekin, D.; Saliba, M.; Zhang, W.; De Bastiani, M.; Petrozza, A.; Herz, L. M.; et al. Charge Selective Contacts, Mobile Ions and Anomalous Hysteresis in Organic-Inorganic Perovskite Solar Cells. *Mater. Horiz.* **2015**, *2*, 315–322.

(43) Calado, P.; Telford, A. M.; Bryant, D.; Li, X.; Nelson, J.; O'Regan, B. C.; Barnes, P. R. F. Evidence for Ion Migration in Hybrid Perovskite Solar Cells with Minimal Hysteresis. *Nat. Commun.* **2016**, *7*, No. 13831.

(44) Luo, Y.; Khoram, P.; Brittan, S.; Zhu, Z.; Lai, B.; Ong, S. P.; Garnett, E. C.; Fenning, D. P. Direct Observation of Halide Migration and Its Effect on the Photoluminescence of Methylammonium Lead Bromide Perovskite Single Crystals. *Adv. Mater.* **2017**, *29*, No. 1703451.

(45) Leijtens, T.; Eperon, G. E.; Barker, A. J.; Grancini, G.; Zhang, W.; Ball, J. M.; Kandada, A. R. S.; Snaith, H. J.; Petrozza, A. Carrier Trapping and Recombination: The Role of Defect Physics in Enhancing the Open Circuit Voltage of Metal Halide Perovskite Solar Cells. *Energy Environ. Sci.* **2016**, *9*, 3472–3481.

(46) Bergmann, V. W.; Guo, Y.; Tanaka, H.; Hermes, I. M.; Li, D.; Klasen, A.; Bretschneider, S. A.; Nakamura, E.; Berger, R.; Weber, S. A. L. Local Time-Dependent Charging in a Perovskite Solar Cell. *ACS Appl. Mater. Interfaces* **2016**, *8*, 19402–19409.

(47) Pockett, A.; Eperon, G. E.; Sakai, N.; Snaith, H. J.; Peter, L. M.; Cameron, P. J. Microseconds, Milliseconds and Seconds: Deconvoluting the Dynamic Behaviour of Planar Perovskite Solar Cells. *Phys. Chem. Chem. Phys.* **2017**, *19*, 5959–5970.

(48) Rutledge, S. A.; Helmy, A. S. Carrier Mobility Enhancement in Poly(3,4-Ethylenedioxythiophene)-Poly(Styrenesulfonate) Having Undergone Rapid Thermal Annealing. *J. Appl. Phys.* **2013**, *114*, No. 133708.

(49) Motta, C.; El-Mellouhi, F.; Sanvito, S. Charge Carrier Mobility in Hybrid Halide Perovskites. *Sci. Rep.* **2015**, *5*, No. 12746.

(50) Von Hauff, E.; Dyakonov, V.; Parisi, J. Study of Field Effect Mobility in PCBM Films and P3HT:PCBM Blends. *Sol. Energy Mater. Sol. Cells* **2005**, *87*, 149–156.

(51) Gelmetti, I.; Cabau, L.; Montcada, N. F.; Palomares, E. Selective Organic Contacts for Methyl Ammonium Lead Iodide (MAPbI<sub>3</sub>) Perovskite Solar Cells: Influence of Layer Thickness on Carriers Extraction and Carriers Lifetime. *ACS Appl. Mater. Interfaces* **2017**, *9*, 21599–21605.

(52) Iftiqar, S. M.; Kim, J. S.; Yi, J. Investigation of Highly Efficient Methyl Ammonium Lead Halide Perovskite Solar Cell with Non-Textured Front Surface. *Optik* **2017**, *148*, 54–62.

(53) Du, T.; Xu, W.; Daboczi, M.; Kim, J.; Xu, S.; Lin, C.-T.; Kang, H.; Lee, K.; Heeney, M. J.; Kim, J.-S.; et al. P-Doping of Organic Hole Transport Layers in p-i-n Perovskite Solar Cells: Correlating Open-Circuit Voltage and Photoluminescence Quenching. *J. Mater. Chem. A* **2019**, *7*, No. 18971.